Journal of Alloys and Compounds 495 (2010) 548–551

Contents lists available at ScienceDirect

Journal of Alloys and Compounds

journal homepage: www.elsevier.com/locate/jallcom

Nanostructured ceramic materials: Applications in gas sensors and solid-oxide fuel cells

D.G. Lamas, M.F. Bianchetti, M.D. Cabezas, N.E. Walsöe de Reca*

CINSO (Centro de Investigaciones en Sólidos), CONICET-CITEFA, Juan B. de La Salle 4397, (B1603ALO) Villa Martelli, Pcia. de Buenos Aires, Argentina

ARTICLE INFO

Article history:
Received 29 July 2008
Received in revised form 29 April 2009
Accepted 4 October 2009
Available online 13 October 2009

Keywords:
Nanostructured materials
Ceramics
Semiconductors
Fuel cells
Chemical synthesis

ABSTRACT

Two applications of nanostructured ceramic materials developed at CINSO in recent years are reviewed, including the synthesis and properties of these materials:

(i) Application of nanostructured SnO_2-based semiconductors for gas sensors, showing the increase of their sensitivity and the decrease of their operating temperature if the sensor is built with nanomaterials in comparison to sensors prepared with conventional microcrystalline materials. The sensing mechanism is discussed in order to explain the different behavior.
(ii) Application of nanocrystalline ZrO_2–CeO_2 solid solutions as novel anodes for solid-oxide fuel cells operated using hydrocarbons as fuel. Other applications of nanoceramics in these devices, recently investigated at CINSO, are also discussed.

1. Nanostructured ceramic semiconductors for gas sensors

Gas sensors built with pure or doped SnO_2 semiconductors (SCs) are based on the variation of their surface resistance. Under air atmosphere, the SC reacts with O_2, forming several oxygen adsorbates (such as O^-, O_2^- and O^{2-}) at its surface and grain boundaries [1]. In the case of *n*-type SC, these adsorbates form a space–charge region, resulting in an electron-depleted surface layer due to the electron transfer to the adsorbates as follows:

$$1/2O_2(g) + 2e^- \leftrightarrow O^-(\text{adsorb.}) \quad (1)$$

The depth of the space–charge (L) is a function of the surface coverage of O_2 adsorbates and the intrinsic electron concentration in the bulk. Then, the resistance of the *n*-type SC is high because a potential barrier to electronic conduction is formed at each grain boundary [2]. If the sensor is exposed to a reducing gas as CO, the oxygen adsorbates react with the gas and they are consumed until a lower steady-state surface coverage is established. In the case of O^- adsorbates, the following reaction takes place:

$$CO(g) + O^-(\text{adsorb.}) \leftrightarrow CO_2(g) + e^- \quad (2)$$

As a consequence, the potential barrier height decreases and a drop in the resistance is produced. The variation of the resistance is the characteristic magnitude of the gas sensor:

$$\Delta\rho = ne\,\Delta L \quad (3)$$

where n is the electron density, e is the electron charge and ΔL is the change of space–charge thickness. The sensitivity (S) of the sensor is defined as:

$$S = \frac{R_{air}}{R_{air+gas}} \quad (4)$$

where R_{air} and $R_{air+gas}$ are the resistance in air and in the mixture of air and reducing gas, respectively. S mainly depends on the reactivity of O_2 adsorbates and it is a function of the reducing gas and the working temperature (T_w) of the sensor. For microcrystalline SC materials, the optimal T_w is typically in the range of 300–450 °C [1,2].

Gas sensors to detect CO(g) [3], VOCs (volatile organic compounds) [4] and H_2 [5] were built at CINSO with micro- and nanocrystalline SnO_2. It was observed that S of sensors built with nanocrystalline material is much higher and the optimal T_w can be significantly reduced. For example, in the case of hydrogen sensors, we observed that S increases 30–37% and the optimal T_w decreased from 350–450 °C to 180–220 °C for sensors built with micro- and nanomaterials, respectively [6]. These results can be understood in terms of a simple model for grain size effects [1]. Assuming that the SC material consists of uniform grains with grain size D connected by grain boundaries, the core exhibits a low resistance, while the space–charge region, of thickness L, has a high resistance. For

* Corresponding author. Tel.: +54 11 4709 8158; fax: +54 11 4709 8158.
E-mail address: walsoe@citefa.gov.ar (N.E.W. de Reca).

0925-8388/$ – see front matter © 2009 Elsevier B.V. All rights reserved.
doi:10.1016/j.jallcom.2009.10.014

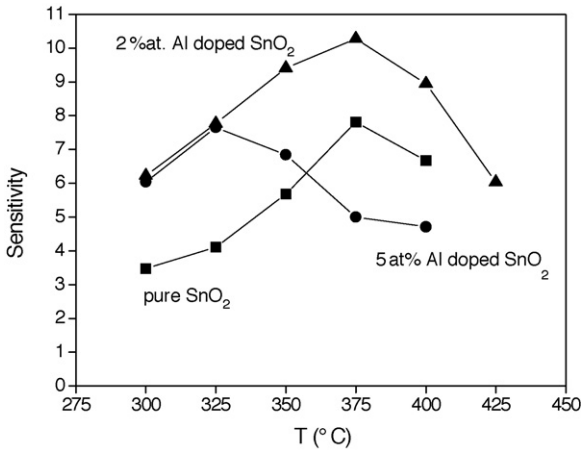

Fig. 1. Sensitivity of nanostructured pure, 2 at.% and 5 at.% Al-doped SnO_2 as a function of working temperature for 200 ppm CO in air.

$D \gg 2L$, the grain boundaries are the only sensitive region and control the sensing properties. Differently, if $D \geq 2L$, there is a control of necks, while for $D \ll 2L$ almost the whole grain can react with the gas, being easy to conclude that S strongly increases as grain size decreases.

Doping of SnO_2 with trivalent cations enables to increase the response since the carrier concentration becomes lower and, consequently, L increases [1,2]. Since the solubility of Al in the SnO_2 lattice is very small, we investigated the possibility of increasing the solubility by synthesizing Al-doped SnO_2 nanopowders by a nitrate–citrate gel-combustion route [3]. This route was previously investigated and optimized at CINSO for the synthesis of SnO_2 nanopowders [6,7] and we chose it in this case because, in other ceramic systems, it probed to increase the solubility limit of doping elements, in a metastable condition, while retaining the compositional homogeneity of the materials [8,9]. This is due to the fact that the material is obtained from the rapid disintegration of a homogeneous precursor gel, so the system cannot evolve towards its equilibrium state. In Fig. 1, the response of pure, 2 at.% and 5 at.% Al-doped SnO_2 is plotted as a function of T_W for 200 ppm CO in air. Comparing the response of 2 at.% Al-doped SnO_2 and pure SnO_2 sensors, it can be observed that the first exhibited higher S for the whole temperature range. The maximum value was of $S \cong 8$ for pure SnO_2 and $S = 10$ for 2 at.% Al-doped SnO_2 and the optimal T_W was similar for both types of sensors, of about 375 °C. However, 5 at.% Al-doped SnO_2 sensors exhibited a lower optimal T_W, of about 325 °C, and $S = 8$. The decrease in the optimal T_W can be assigned to a shift of the characteristic formation temperature of adsorbates by the incorporation of Al in the SnO_2 lattice. Our results showed that the gel-combustion method enables to increase the Al solubility in nanocrystalline SnO_2 in comparison with the co-precipitation method with a simultaneous decrease of crystallite size [3], thus allowing to reduce the optimal T_W.

We also developed a new route for the synthesis of pure SnO_2 nanopowders starting from $SnCl_2{\cdot}2H_2O$ by a vigorous oxidation method [5], obtaining an initial crystallite size of 1–2 nm and a final size of 5–6 nm after sintering. Fig. 2 shows S as a function of T_W for a H_2 sensor prepared using this nanopowder. S resulted 30–35% higher than that of sensors built with micro-SnO_2 synthesized with the usual calcination method and the optimal T_W resulted of 180–200 °C. Differently, commercial sensors with microcrystalline SnO_2 operate in a range 350–450 °C.

In addition to the advantage of the use of a nanostructured sensing material, an innovative commutative heater and measurement circuit, developed at Semiconductors Lab of CITEFA using MEMS technique (similar to heating circuits used for thin film sensors

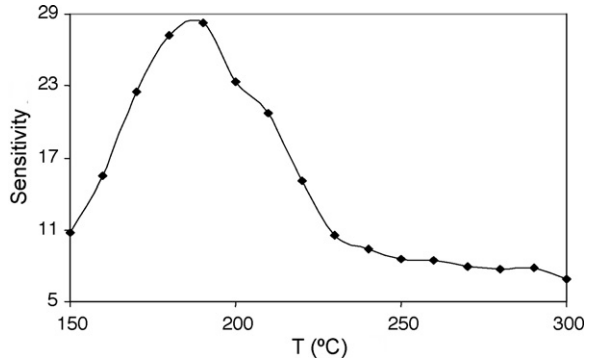

Fig. 2. Sensitivity versus working temperature of nanostructured SnO_2 sensor for H_2 in air.

[10]), was incorporated to the H_2 sensor because of the lower power required for sensor operation [11].

2. Nanostructured ceramic materials for solid-oxide fuel cells

Fuel cells are electrochemical devices for power generation in which the chemical energy of a reaction, usually water formation from H_2 and O_2, is directly converted into electrical energy. In comparison to other types of fuel cells, solid-oxide fuel cells (SOFCs) have the important advantage of their fuel flexibility, since hydrocarbons, such as CH_4, can be used as fuels instead of H_2.

Conventional SOFCs employ ceramic electrolytes, usually Y_2O_3-stabilized ZrO_2 (YSZ), that exhibit high oxide-ion conductivity at high temperature. The reduction reaction of O_2 to O^{2-} is produced at the cathode and manganites such as (La;Sr)MnO_3 (LSM) are generally used to catalyze it. Finally, fuel oxidation takes place at the anode and Ni-based materials are widely employed in order to catalyze the internal reforming of CH_4 in presence of H_2O or CO_2:

$$CH_4 + H_2O \rightarrow 3H_2 + CO \quad (5a)$$

$$CH_4 + CO_2 \rightarrow 2H_2 + 2CO \quad (5b)$$

The resulting gases, H_2 and CO, react with the O^{2-} ions coming from the electrolyte to produce water and CO_2.

The main difficulty of these conventional SOFCs is their high T_W, usually in the range 900–1000 °C, due to the fact that the above-mentioned materials have high efficient only at high temperatures. However, high T_W causes degradation problems due to thermal cycling or diffusion at interfaces and requires the use of expensive interconnection materials. For these reasons, significant effort has been devoted to find new materials that exhibit high performance at lower temperatures, giving rise to the intermediate-temperature SOFCs (IT-SOFCs) which operate at 500–700 °C. Excellent materials for solid electrolytes have been proposed, such as Sm_2O_3, Gd_2O_3 or Y_2O_3-doped CeO_2 or (La;Sr)(Ga;Mg)O_3. In the case of the cathode, cobaltites and cobalto-ferrites (for example, (La;Sr)CoO_3, (Sm;Sr)CoO_3, (La;Sr)(Co;Fe)O_3, etc.) with perovskite-type structure exhibit excellent electrocatalytical properties for oxygen reduction. The main problem relies in the anode, particularly for operation with hydrocarbons as fuels, since internal reforming is only efficient at high temperatures. Consequently, new concepts are being considered: SOFCs working by direct oxidation of hydrocarbons [12–15], which operate without incorporating water or CO_2, and the one-chamber SOFCs [16–21]. In the following, we will discuss this last type of SOFCs.

Usually, fuel and O_2(air) are separated in two chambers. However, Hibino et al. [16–19] have proposed "one-chamber" SOFCs that operate in mixtures of hydrocarbons and air. These fuel cells rely on the use of highly selective anode and cathode materials for

fuel oxidation and oxygen reduction reactions, respectively. In the anode, instead of the internal reforming, the ambient O_2 is used to produce the partial oxidation of the hydrocarbon. For CH_4, this reaction is:

$$CH_4 + 1/2O_2 \rightarrow 2H_2 + CO \quad (6)$$

which has been proposed to proceed through the following sequence of reactions [16]:

$$CH_4 + 2O_2 \rightarrow 2H_2O + CO_2 \quad (7a)$$

$$CH_4 + H_2O \rightarrow 3H_2 + CO \quad (7b)$$

$$CH_4 + CO_2 \rightarrow 2H_2 + 2CO \quad (7c)$$

One-chamber SOFCs have great relevance since they allow the simplification of the cell design (with the consequent reduction in volume, weight and cost of the device). Besides, different from the case of the internal reforming, the partial oxidation of hydrocarbons can be catalyzed at intermediate temperatures. Since the feasibility of one-chamber SOFCs is still under evaluation, this new concept is under intense study at CINSO [20,21].

One important goal of the research work carried out at CINSO was to propose new anodes based on composites of NiO and ZrO_2–CeO_2 solid solutions [21]. The interest on these anodes relies on the fact that ZrO_2–CeO_2 materials are mixed ionic/electronic conductors in reducing atmosphere and, therefore, fuel oxidation is produced on its entire surface, while it only occurs in the [anode/electrolyte/gas] interphase (triple-phase boundaries) for electronic conductors. More interestingly, nanostructured mixed conductors should exhibit even more reaction sites in comparison to conventional microcrystalline materials due to the increase of the specific surface area. This idea has been recently exploited at CINSO to develop high-performance cathodes [22]. Besides, in a previous work [23], we showed the excellent catalytic properties for CH_4 oxidation of nanocrystalline ZrO_2–50 mol%, 70 mol% and 90 mol% CeO_2 solid solutions exhibiting the t′-form of the tetragonal phase, the t″-form of the tetragonal phase and the cubic phase, respectively. The synthesis of these nanocrystalline ZrO_2–CeO_2 solid solutions by gel-combustion routes, their crystal structure and the retention of metastable forms of the tetragonal phase in these materials have also been subjects of intense investigation at CINSO [8,9,24–26].

In order to study the performance of the novel NiO/ZrO_2–CeO_2 anodes, we constructed and evaluated one-chamber SOFCs with YSZ electrolytes, LSM cathodes and different anodes: NiO and NiO/ZrO_2–50 mol%, 70 mol% and 90 mol% CeO_2 anodes [21]. These cells were tested under CH_4/air mixtures with CH_4:O_2 ratios between 1:1 and 2:1. Fig. 3a shows the discharge curves obtained for anodes of NiO and NiO/ZrO_2–70 mol% CeO_2 composites. Fig. 3b shows the curves of power density as a function of the current density of both cells. Both curves were obtained at 950 °C for mixtures with CH_4/O_2 ratio of 1:1, which proved to be the optimum mixture for both cells. One-chamber SOFCs with NiO anode, already studied in the literature [16], allowed us to optimize the cell preparation and operating conditions. Despite the fact that the peak power density reported by Hibino and coworkers (121 W/cm^2) was not reached, the value obtained in our study (39 mW/cm^2) is acceptable considering that the electrodes were synthesized using inexpensive chemicals of analytical reagent grade.

For the NiO/ZrO_2–CeO_2 anodes, adhesion problems were found, not only during the cell preparation but also under operation. This effect is known in the literature and it is due to the lattice expansion that appears when the Ce changes from Ce^{4+} to Ce^{3+} in a reducing atmosphere [27]. These problems were more pronounced in the case of ZrO_2–90 mol% CeO_2 solid solutions. On the other hand, for NiO/ZrO_2–50 mol% CeO_2 composites, a good adhesion was only achieved for sintering temperatures of about 1050 °C. Since

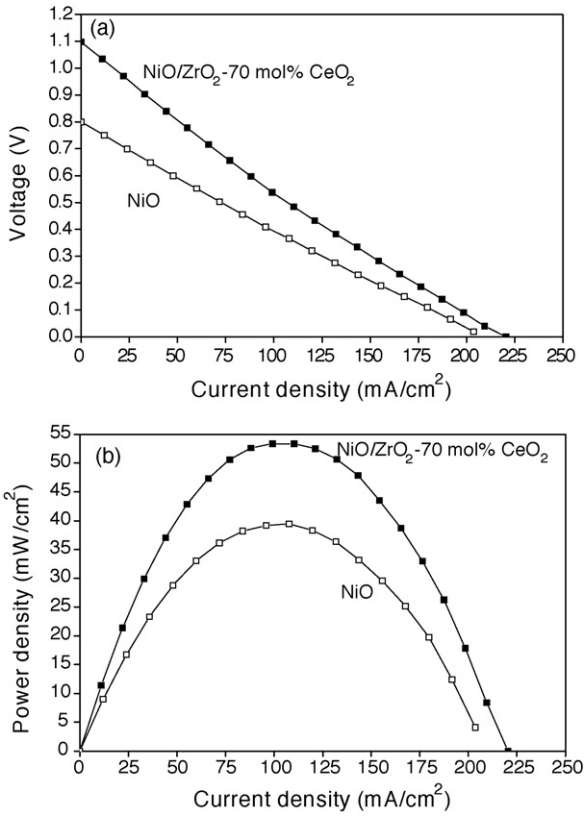

Fig. 3. Voltage versus current density (a) and power density versus current density (b) for one-chamber SOFCs with NiO and NiO/ZrO_2–70 mol% CeO_2 anodes, operated at 950 °C under a CH_4 + air mixture with CH_4:O_2 ratio of 1:1.

ZrO_2–50 mol% CeO_2 nanopowders synthesized by gel-combustion lose their compositional homogeneity at temperatures of 950 °C or higher [9], the performance of composites with this solid solution was not investigated in this work. Thus, only the NiO/ZrO_2–70 mol% CeO_2 composite exhibited adequate properties for application as anode. This anode was sintered at 1000 °C during 1.5 h to avoid the degradation of the solid solution [9].

As it can be observed in Fig. 3b, the NiO/ZrO_2–70 mol% CeO_2 composite anode has a better performance than that of NiO, reaching a peak power density of 53 mW/cm^2, which means an increase of 36%. This improvement in the performance of the one-chamber SOFC is due to the excellent catalytic properties of the composites for partial oxidation of CH_4. The mechanism of the partial oxidation reaction is probably that described by reactions (7a)–(7c): ZrO_2–70 mol% CeO_2 solid solution promotes the total oxidation of CH_4 in presence of O_2 (reaction (7a)), and the formation of water and CO_2 favors the reforming of non-reacted CH_4 in the presence of NiO catalysts (reactions (7b) and (7c), respectively), producing H_2 and CO in a more efficient way, thus increasing the power density of the fuel cell.

This application of ZrO_2–CeO_2 nanoceramics as anodes in SOFCs combines two interesting properties of nanomaterials: their enhanced properties due to the high specific surface area (in this case, the greater number of active sites for fuel oxidation) and the retention of a metastable phase with high performance (the excellent catalytic properties of ZrO_2–CeO_2 solid solutions exhibiting the tetragonal phase). However, this study also shows the limitations of the use of nanomaterials in SOFCs: if high temperatures are required for preparation or operation of the cell, grain growth takes place thus affecting their properties. For this reason, we suggested their application in IT-SOFCs and, in order to evaluate this novel concept, several nanostructured ceramic materials are under

study at CINSO, such as high-performance electrodes [22] and high-conductivity solid electrolytes [28,29]. In the last case, we have demonstrated the enhanced ionic conductivity of nanostructured CeO_2-based ceramics, mainly due to the raise of the parallel grain boundary conductivity in the nanostructured samples, coupled to an increase of the grain boundary ionic diffusivity with decreasing grain size [28,29]. These works show the wide diversity of properties and applications of nanostructured ceramic materials, which deserves to continue under intense investigation in the near future.

Acknowledgements

The authors are indebted to YPF Foundation (2003 Repsol-YPF Award and several fellowships given to young researchers), Agencia Nacional de Promoción Científica y Tecnológica (Argentina, PICT No. 14268 and PICT No. 38309), CONICET (Argentina, PIP No. 6559), the scientific collaboration agreements CNPq-CONICET and CAPES-SECyT (Brazil-Argentina), CNPq (Brazil, PROSUL program 490289/2005-3), and Centro Latinoamericano de Física (Latinoamerican Centre of Physics, CLAF).

References

[1] N. Yamazoe, J. Fuchigami, M. Kishikawa, T. Seiyama, Surf. Sci. 86 (1979) 335.
[2] Y. Shimizu, M. Egashira, MRS Bull. 24 (1999) 18.
[3] M.D. Cabezas, R. Baby, E.D. Cabanillas, D.G. Lamas, N.E. Walsöe de Reca, J. Argen. Chem. Soc. 93 (2005) 69.
[4] M.F. Bianchetti, N.E. Walsöe de Reca, Application for Argentine Patent (in process).
[5] M.F. Bianchetti, M.E. Rapp, R.E. Juárez, N.E. Walsöe de Reca, Application for Argentine Patent (in process).
[6] L.B. Fraigi, D.G. Lamas, N.E. Walsöe de Reca, Nanostruct. Mater. 11 (1999) 311.
[7] L.B. Fraigi, D.G. Lamas, N.E. Walsöe de Reca, Mater. Lett. 47 (2001) 262.
[8] D.G. Lamas, N.E. Walsöe de Reca, J. Mater. Sci. 35 (2000) 5563.
[9] D.G. Lamas, G.E. Lascalea, R.E. Juárez, E. Djurado, L. Pérez, N.E. Walsöe de Reca, J. Mater. Chem. 13 (2003) 904.
[10] G. Cardinali, L. Dori, M. Fiorini, I. Sayago, G. Faglia, C. Perego, G. Sberveglieri, V. Liberali, F. Maloberti, D. Tonetto, Annu. Rep. CNR-LAMEL (Italy) (1998) 71.
[11] L.T. Alaniz, C.L. Arrieta, M.F. Bianchetti, C.A. Gillari, J.F. Giménez, H.A. Lacomi, D.F. Valerio, N.E. Walsöe de Reca, Argentine Patent P-070105987 (2007).
[12] B.C.H. Steele, Nature 400 (1999) 619.
[13] E. Perry Murray, T. Sai, S.A. Barnett, Nature 400 (1999) 649.
[14] S. Park, J.M. Vohs, R.J. Gorte, Nature 404 (2000) 265.
[15] S. McIntosh, R.J. Gorte, Chem. Rev. 104 (2004) 4845.
[16] T. Hibino, S. Wang, S. Kakimoto, M. Sano, Solid State Ionics 127 (2000) 89.
[17] T. Hibino, A. Hashimoto, T. Inoue, J. Tokuno, S. Yoshida, M. Sano, Science 288 (2000) 2031.
[18] T. Hibino, A. Hashimoto, M. Yano, M. Suzuki, S. Yoshida, M. Sano, J. Electrochem. Soc. 149 (2002) A133.
[19] M. Yano, A. Tomita, M. Sano, T. Hibino, Solid State Ionics 177 (2007) 3351.
[20] M.D. Cabezas, D.G. Lamas, M.G. Bellino, R.O. Fuentes, N.E. Walsöe de Reca, ECS Trans. Solid Oxide Fuel Cells 7 (2007) 955.
[21] D.G. Lamas, M.D. Cabezas, I.O. Fábregas, N.E. Walsöe de Reca, G.E. Lascalea, A. Kodjaian, M.A. Vidal, N.E. Amadeo, S.A. Larrondo, ECS Trans. Solid Oxide Fuel Cells 7 (2007) 961.
[22] M.G. Bellino, J.G. Sacanell, D.G. Lamas, A.G. Leyva, N.E. Walsöe de Reca, J. Am. Chem. Soc. 129 (2007) 3066.
[23] S. Larrondo, M.A. Vidal, B. Irigoyen, A.F. Craievich, D.G. Lamas, I.O. Fábregas, G.E. Lascalea, N.E. Walsöe de Reca, N. Amadeo, Catal. Today 107–108 (2005) 53.
[24] G.E. Lascalea, D.G. Lamas, L. Pérez, E.D. Cabanillas, N.E. Walsöe de Reca, Mater. Lett. 58 (2004) 2456.
[25] D.G. Lamas, R.O. Fuentes, I.O. Fábregas, M.E. Fernández de Rapp, G.E. Lascalea, J.R. Casanova, N.E. Walsöe de Reca, A.F. Craievich, J. Appl. Cryst. 38 (2005) 867.
[26] G.E. Lascalea, D.G. Lamas, E. Djurado, E.D. Cabanillas, N.E. Walsöe de Reca, Mater. Res. Bull. 40 (2005) 2029.
[27] A. Trovarelli, Catal. Rev. Sci. Eng. 38 (1996) 439.
[28] M.G. Bellino, D.G. Lamas, N.E. Walsöe de Reca, Adv. Funct. Mater. 16 (2006) 107.
[29] M.G. Bellino, D.G. Lamas, N.E. Walsöe de Reca, Adv. Mater. 18 (2006) 3005.